Retrieval of High-Resolution Aerosol Optical Depth (AOD) using Landsat 8 imageries over different LULC classes over a City along Indo-Gangetic Plain, India

Rohit Kumar Singh
Indian Institute of Technology Kharagpur
A. N. V. Satyanarayana (anvsatya@coral.iitkgp.ac.in)
Indian Institute of Technology Kharagpur
P. S. Hari Prasad
Indian Institute of Technology Kharagpur

Research Article

Keywords: AOD, AERONET, MODIS, Land use Land cover

Posted Date: October 3rd, 2023

DOI: https://doi.org/10.21203/rs.3.rs-3376218/v1

Abstract

Aerosol Optical Depth (AOD) serves as a crucial indicator for assessing regional air quality by quantifying aerosol levels in the atmosphere. While various satellite methods exist for estimating AOD, the spatial resolution of established AOD products is often limited. However, obtaining higher-resolution AOD data is essential for gaining a deeper understanding of regional and urban air pollution issues. To address this issue, we retrieved high-resolution AOD over Kanpur (26.4499° N, 80.3319° E), located in the Indo-Gangetic Plain (IGP) region using Landsat 8 imageries. We have used Landsat 8 imagery and the SEMARA algorithm, which combines SARA (Simplified Aerosol Retrieval Algorithm) and SREM (Simplified and Robust Surface Reflectance Estimation). Our approach leveraged the green band of the Landsat 8, resulting in an impressive spatial resolution of 30 meters. This methodology was applied over the period from 2014 to 2022 and rigorously validated with available AERONET observations. The retrieved AOD is in good agreement with high correlation coefficients (r) of 0.997, a low root mean squared error (RMSE) of 0.035, and root mean bias (RMB) of -4.91%. Furthermore, we conducted a comprehensive comparison with downscaled MODIS (MCD19A2) AOD products across various land classes for cropped and harvested period of agriculture cycle with different land use and land cover classes. The SEMARA approach proved to be more effective for AOD retrieval on brighter surfaces within the barren and built-up land categories for harvested period. This methodology holds great potential for monitoring aerosols over bright urban areas.

1. Introduction

Aerosols are often made up of liquid and solid particles that are suspended in the air and are a result of both anthropogenic activity and natural emissions. Aerosols include smoke, volcanic ash, dust, sea salt, and particulate pollution. By limiting air visibility, aerosols have an impact on not just the climate system of earth but also on human health and the hydrological cycle (Koren et al., 2012; Pope III et al., 2009). The Aerosol Optical Depth (AOD) is a measurement of the amount of solar light that is extinguished (scattering and absorption) due to aerosol particles (Acharya & Sreekesh, 2013; Arafath et al., 2015; Van de Hulst, 1948). It's a one-dimensional quantity that refers to the amount of aerosol in the vertical column of the atmosphere above the observation point. AOD is one of the most essential optical parameters of aerosol utilised in radiative transfer calculations (Ge et al., 2011; Ramachandran et al., 2012).

Monitoring the AOD can be done in two main methods. One approach involves the use of ground-based sun photometers, whereas the alternative method relies on sensors installed on satellite platforms. Beginning in the middle of the 1970s, aerosol characteristics were determined through satellite measurements (Stowe et al., 1992). Currently, there are numerous ways to invert the AOD, which is an optical parameter that indicates how much an aerosol stops light from passing through (Hadjimitsis, 2009), including the Deep Blue (DB) approach (Hsu et al., 2013), Dark Target (DT) approach (Kaufman & Sendra, 1988; Remer et al., 2020), multi-angle polarization method (Chen et al., 2015), and the Structure-Function or Contrast Reduction (SFCR) method (Tanré et al., 1988). Although there are several methods to obtain AOD through satellite observations, there are some shortcomings that hinder the study of aerosols

on the local scale, like the limited spatial resolution of well-established AOD imageries, which is up to 1 km for MODIS MAIAC product MCD19A2. In order to better comprehend the issue of urban air pollution, it is necessary to examine aerosol products with higher spatial resolutions. Several researchers have employed Landsat 8 imagery and MODIS09A1 surface reflectance datasets to estimate AOD at a 30-meter resolution by utilizing a lookup table (LUT) derived from the radiative transfer model (Jin et al., 2021; Kang et al., 2022; Lin et al., 2021). Liang et al., (2022) retrieved AOD at a higher resolution with the help of machine learning models. Simplified Aerosol Retrieval Algorithm (SARA) has been used in multiple studies (Bilal et al., 2013a; Bilal & Qiu, 2018; Rahman & Haque, 2022), which shows a greater correlation with real data values obtained from AERONET stations, and it does not require look-up table, unlike previous algorithms. In this study, we have used the SEMARA algorithm, which is a combination of SARA and SREM (Simplified and Robust Surface Reflectance Estimation). SREM has been used to calculate the surface reflectance (Bilal et al., 2019a), which was ultimately used in the SARA algorithm to calculate AOD values at 30m resolution (Bilal et al., 2013b).

The current retrieval and analysis of aerosol products were conducted over the Kanpur region of the Indo-Gangetic Plain (IGP) in southern Asia taking into account the wide range of aerosol types and different aerosol loadings that persist throughout the entire year. The IGP has shown significant seasonal and interannual fluctuation in aerosols because of local climatology, atmospheric dynamics, and emissions of both natural and man-made aerosols (Kaskaoutis et al., 2013; Nair et al., 2007). According to Payra et al. (2021), Kolkata witnessed the most notable rise in AOD percentage from 2007 to 2018 at 39%, with Delhi showing a 27.34% increase, followed by Chennai and Jaipur, both with a 26.30% increase. Gupta (2008) found that due to the large scale of industrial activity and transportation fleet, the level of PM10 is five to six times greater than the safe level in Kanpur's central areas. Particulate matter pollution is influenced by the presence of fine and coarse aerosol particles in the atmosphere, causing reduced regional visibility, increased occurrences of haze, and numerous impacts on the local ecosystem, living conditions, and human health (Pope et al., 1995; Zhang et al., 2019).

The IGP's large inter-seasonal variance in surface reflectance makes it difficult to retrieve good quality aerosol data consistently (Mhawish et al., 2017). Uncertainties in the retrieval of AOD in this region are also caused by factors contributing to variations in aerosol single scattering albedo (SSA) include the presence of dense vegetation, whether accompanied by a different brightness of the soil surfaces, changes induced by intense dust storms, especially in the pre-monsoon period, and the prevalence of fine particles, particularly during the post-monsoon to winter season (Tripathi et al., 2005). Tracking aerosol characteristics above complex and mixed bright urban terrains, as observed in Kanpur, presents notable challenges, particularly during periods of elevated aerosol loading. This complexity is further compounded by the proximity of these urban areas to agricultural fields, which undergo significant changes in land use patterns over the course of a year, transitioning between the cropped and harvested periods.

Therefore, recognizing the necessity of retrieving the high resolution AOD over Kanpur region of IGP to study the city scale phenomenon. This study involves the retrieval of high-resolution AOD through the

implementation of the SEMARA algorithm. The validation and assessment of its performance have been conducted by comparing the results with AERONET observations. Furthermore, a thorough comparison has been undertaken with the MODIS (MCD19A2) AOD product, which was downscaled to achieve a spatial resolution of 30 meters. This study offers a first comparative examination of SEMARA retrieved AOD (30m x 30m) and MODIS (MCD19A2) AOD over a station of IGP.

2. Study Region

The majority of northern India's land is covered by the Indo-Gangetic Plain (IGP), which is a significant hub for economic, industrial, and agricultural activity and has the nation's greatest aerosol loading (Shukla et al., 2020). Kanpur (26.4499° N, 80.3319° E) is a city located in the central part of the Indo-Gangetic region. Kanpur is an important industrial city known for its leather, textiles, and chemicals industries (Gupta, 2008). It was named the most polluted city in the world in terms of annual mean PM2.5 concentrations by the WHO Ambient Air Quality Database for 2018 (The et al., 2018). According to the 2011 census, the population of Kanpur is 34,70,334. The pollution is caused by various factors, including vehicular emissions, industrial pollution, and crop burning in nearby regions (Murari et al., 2015). Although Kanpur, being a big city with a high population density and a lot of factories, releases a lot of aerosol particles annually, which has led to a steady rise in the pollution levels in the region. The study area encompasses the Kanpur tehsil within the Kanpur district, spanning an area of 1122 square km (Fig. 1). The research was undertaken during 2014 to 2022.

3. Data Used

3.1 AERONET Observations

The Aerosol Robotic Network (AERONET), used to verify AOD retrieval techniques from satellites, gathers local AOD values by measuring the solar direct radiance using the sun-photometer. AOD Version 3 Level 1.5 observations have been obtained through the AERONET station (26.51278° N, 80.23164° E) on the IIT Kanpur campus (Fig. 1) from the website (https://aeronet.gsfc.nasa.gov/) for the period of 2014 to 2022.

3.2 MODIS Datasets

The MAIAC (MCD19A2) products from the MODIS collection 6.1 dataset, which are accessible through the National Aeronautics and Space Administration (NASA; https://ladsweb.modaps.eosdis.nasa.gov/), were used for the comparison and validation of SEMARA generated AOD. which is the combined Terra and Aqua product with a 1 km spatial resolution and one day of temporal resolution. It measures AOD at 0.47 μm (blue band), and 0.55 μm (green band); the green band was utilized in this study. For the study area covering the Kanpur region, a MODIS product that was provided in a sinusoidal grid (H25V06) was utilized.

3.3 LANDSAT Observations

The Landsat 8 satellite is equipped with the sensor Operational Land Imager (OLI), which provides eight bands covering a range from visible to short-wave infrared wavelengths, all with a spatial resolution of 30 meters. The United States Geological Survey (USGS; https://earthexplorer.usgs.gov/) provided 98 OLI pictures after filtering out the cloud mask which was set to < 30% of cloud cover from Landsat 8 taken within the scene (path/row: 144/42) between January 2014 and December 2022 for this study.

4. Methodology

4.1 Retrieval of AOD

In this study, the SEMARA technique (Bilal et al., 2022) was used to retrieve AOD utilizing data from the green band of Landsat 8 OLI. Radiative Transfer Model (RTM) equations were applied to LANDSAT imageries to recover AOD at spatial resolution of 30m. Surface reflectance (SR), solar and sensor geometry, and TOA (Top of Atmosphere) reflectance data were obtained from LANDSAT imagery using USGS Earth Explorer. The SEMARA algorithm was applied employing two key equations. The first equation utilized was the SREM equation, used for calculating surface reflectance (Bilal et al., 2019). The second equation employed was the SARA equation, utilized to estimate AOD (Bilal et al., 2013a). The detailed methodology and calculations involved in the SEMARA algorithm have been shown in Fig. 2.

The AOD values observed by AERONET's sun-photometer were extrapolated to 550 nm through the utilization of the Ångström exponent (α), derived from the AOD values at 440 and 675 nm ($\alpha_{440-675}$) in conjunction with the AOD at 500 nm. Geographic heterogeneity resulting from air motion was considered, and AERONET AOD data (requiring a minimum of three available observations) were averaged within a 120-minute time window centered around the Landsat 8 overpass periods in Kanpur. The single scattering albedo (ω_0) and asymmetry factor (g) are calculated using sun-photometer observed AOD (τ_A). This is accomplished by adjusting ω_0 and g within the specified ranges of 0 to 1 and we took the corresponding ω_0 and g which is nearest neighbour to the AERONET observations in contour of AOD. The chosen ω_0 and g values are employed to estimate the AOD in areas distant from the AERONET location. These parameters hold true for a specific visual scene in terms of spatial consistency. The calculated ω_0 and g may not provide an entirely accurate representation of the true optical characteristics of aerosols due to the simplifications inherent in the SARA approach (Bilal et al., 2013a).

4.2 Validation with AERONET Observations and Comparison with MODIS AOD Product

To assess the accuracy of the retrieved AOD, comparisons were made with AERONET observations. The SEMARA-retrieved AOD values were averaged over a 3 x 3-pixel area, with the AERONET station at the centre. For data to be included in the average, a minimum of 2 out of the 9 pixels needed to have available data.

The AOD data extracted from the MODIS (MCD19A2) product, which is a combined Terra and Aqua dataset, possessed a geographical resolution of 1 km. Given its sinusoidal projection, a conversion to the UTM projection was carried out to align with the projection used for Landsat 8 imagery. Additionally, the MODIS AOD product was downscaled to a 30-meter resolution utilizing the nearest neighbour interpolation method. This step was taken to align the resolution of the MODIS AOD data with that of the AOD retrieved using the SEMARA algorithm. Comparison with MAIAC derived AOD product has been done in three way. Overall mean of MAIAC and SEMARA AOD has been compared. Also, comparison of SEMARA retrieved AOD has been done for the different land cover types. For this analysis, the LULC (Land Use Land Class) map has been used as a proxy. The LULC map was generated using different bands of LANDSAT images using the maximum likelihood method (Sultana & Satyanarayana, 2018, 2020). The Kanpur region has been classified into four land types: (i) Barren Land, (ii) Built-up Land, (iii) Vegetation, and (iv) Water bodies. Furthermore, an investigation encompassing all four land classes was conducted for both the cropped and harvested agricultural periods. The performance assessment of the SEMARA algorithm was carried out across four distinct aerosol loading ranges: low (AOD ≤ 0.25), moderate (0.25 < AOD ≤ 0.50), high (0.50 < AOD ≤ 0.75), and very high (AOD > 0.75).

4.3 Statistical Analysis

The correlation coefficient (*R*), coefficient of determination (R^2), root mean square error (*RMSE*, Eq. (1)) (Chai & Draxler, 2014), mean absolute error (*MAE*, Eq. (2)) (Hodson, 2022), expected error (*EE*, Eq. (3)) (Karimi et al., 2019), root mean bias (*RMB*, Eq. (4)) (Wei et al., 2017), and fraction of EE (*FOE*, Eq. (5)) (Mi et al., 2007) were employed as statistical indicators to assess comparisons of the retrieved AOD with ground-based AERONET observations and MODIS product.

$$RMSE = \sqrt{\frac{1}{n}\sum_{i=1}^{n}\left(AOD_{(SEMARA)i} - AOD_{(Obs)i}\right)^2}$$

1

Where, AOD_{Obs}. is the Sun photometer's measured AOD and MODIS AOD values;

AOD_{SEMARA} is the SEMARA retrieved AOD.

$$MAE = \frac{1}{n}\sum_{i=1}^{n}\left|AOD_{(SEMARA)i} - AOD_{(Obs)i}\right|$$

2

$$EE = \pm\left(0.05 + 0.15 \times AOD_{(Obs)}\right)$$

3

$$RMB = \frac{\left(\overline{AOD}_{SEMARA} - \overline{AOD}_{Obs}\right)}{\overline{AOD}_{SEMARA}} \times 100$$

4

$$FOE = \frac{(AOD_{SEMARA} - AOD_{Obs})}{|EE|} \quad (5)$$

$$\%EEEnvelope = AOD_{Obs} - |EE| \leq AOD_{SEMARA} \leq AOD_{Obs} + |EE| \quad (6)$$

Where a good match is indicated by |FOE| <1. Values of FOE < 0 and FOE > 0 signify an underestimating and an overestimation, respectively, of satellite retrievals (Levy et al., 2010).

5 Results and Discussion

5.1 Validation of Retrieved AOD

In this study, for the validation purpose we have used AOD values from two sources. First is from AERONET observation which is available at a point location, and second is downscaled MODIS MAIAC AOD product with 30m spatial resolution. As only one AERONET observatory is available in the study area, total 98 collocated AOD data pairs were available. Whereas, after filtering out cloud-affected datasets, a total of 53 collocated data pairs were made available from MAIAC AOD. Table 1 and Fig. 3 show the general statistics for the data distribution of SEMARA retrieved AOD, AERONET observed AOD, and MODIS AOD products.

Table 1
Statistics of AOD's for different retrieval methods, where N denotes the number of days considered in the study for each AOD retrieval method.

Method of Retrieval	N	Mean	Median	Std. Dev.
SEMARA	98	0.5873	0.5322	0.2571
AERONET	98	0.6162	0.5606	0.2565
MODIS	53	0.6168	0.5571	0.2840

Figure 4 represents the scatter plots for the validation of SEMARA retrieved AOD with AERONET observed pointwise AOD (Fig. 4(a)) and satellite MODIS AOD product (Fig. 4(b)). The 1:1 line, EE (Eq. (3)) envelope lines, and regression line are represented in 4 by the dashed (green), solid (black), and solid (red) lines, respectively. The SEMARA 500 m AOD showed a high correlation coefficient (R = 0.997) and low values of RMSE (0.035) and MAE (0.028). The SEMARA AOD and AERONET AOD showed strong agreement, as shown in Fig. 4(a), and nearly all of the observations fall close to the 1:1 line. A good quality of the retrieved AOD is indicated by the fact that 98.98% of the SEMARA-retrieved AOD observations fit inside the confidence envelope (Eq. (6)).

Unlike AERONET observations, MODIS provided AOD for every 1 km of pixels over Kanpur, which was used for detailed validation of SEMARA-retrieved AOD. MODIS AOD, which is retrieved by the MAIAC algorithm, has had its accuracy assessed in several studies all over the globe (Falah et al., 2021; Lyapustin et al., 2018; Mhawish et al., 2019; Tao et al., 2019). We used the MAIAC retrieved AOD for validation since there weren't many AERONET observations over the Kanpur region. Additionally, MODIS provided AOD for each 1km x 1km pixel, which was used for a thorough analysis of the SEMARA approach's performance across different land classes and multiple aerosol loadings after downscaling MODIS AOD to 30m of spatial resolution. After filtering out cloud-affected datasets, a total of 53 collocated data pairs were made available, which were further averaged over the study region and compared. The SEMARA AOD and MODIS AOD showed good agreement (R = 0.779, RMSE = 0.03, and MAE = 0.151). A broad scatter of points is visible in Fig. 4b for SEMARA AOD as a result of both under- and overestimation.

5.2 Efficiency Evaluation over Different Land Classes

The accuracy of the AOD retrieval is significantly impacted by the brightness of the ground surface. Over dark surfaces, The aerosol signal at the top of the atmosphere is significantly more pronounced than that observed over brighter surfaces (Levy et al., 2013; Sayer et al., 2014). In this section, we therefore employ the land use land cover map, which has been classified as barren, built-up, vegetation, and water body, to assess the performance of the retrieved AOD to the different land classes. Beyond Kanpur's city limits, there is a higher concentration of vegetation which is mostly agricultural crops (5), which varies periodically, with more greenery in the cropped seasons (Table 2). As most of the outskirts of Kanpur city is agricultural land, the two LULC maps have been used for cropped (Fig. 5(a-c)) and harvested months (Fig. 5(d-f)) for the years 2015, 2018, and 2021.

Table 2
Percentage area covered by each class for a given year and agricultural cycle.

Class	2015		2018		2021	
	Cropped	Harvested	Cropped	Harvested	Cropped	Harvested
Built-up	39.60	38.19	41.58	40.61	43.35	43.86
Vegetation	52.95	15.33	55.71	18.99	55.62	13.62
Barren/Fallow	7	45.84	2.18	39.76	0.34	39.58
Water Body	0.46	0.65	0.54	0.65	0.69	2.95

Figure 6 and Table 3 represent the data distribution of AOD products for all four land classes. Results suggest that MODIS AOD data has larger spread than that of SEMARA retrieved AOD for all land classes. It may be due to the dependence of the SEMARA algorithm on reference AOD values used for the estimation of g and ω_0.

Table 3
Statistics of SEMARA retrieved AOD's for different land types

	Barren		Built-up		Vegetation		Water	
	MODIS	SEMARA	MODIS	SEMARA	MODIS	SEMARA	MODIS	SEMARA
Mean	0.6201	0.5999	0.6171	0.5897	0.6056	0.5904	0.6258	0.5925
Median	0.5717	0.5887	0.5520	0.5691	0.5487	0.5624	0.5775	0.6012
Std. dev.	0.2811	0.2461	0.2861	0.2493	0.2948	0.2502	0.3012	0.2320

Figure 7 demonstrate that the built-up land class, which consists primarily of city area of Kanpur, is where the SEMARA algorithm better correlated with MODIS AOD product than the land classes of vegetation, barren, and water body. Brighter surfaces of barren and built-up land classes performed better than vegetation areas, as about 63.64%, 61.82%, and 58.18% observations lies in EE envelope for barren, built-up, and vegetation land, respectively.

With approximately 58–66% of the retrieved AOD values falling within the expected error (EE) range, displaying a moderate root mean square error (RMSE) of 0.201 to 0.215, and a low relative mean bias (RMB) ranging from − 2.57% to -5.63%, the SEMARA-retrieved AOD performed well generally over all terrestrial surfaces. These findings imply that the SEMARA technique may retrieve AOD over various terrestrial surface types.

Figure 8 shows the box plots for all four land classes for bias ($AOD_{SEMARA} – AOD_{MODIS}$). It shows an overall underestimation of SEMARA retrieved AOD values for all classes. For built-up and water bodies, it may be due to an overestimation of surface reflectance in SREM, which results in a comparatively higher underestimation of AOD values than barren and vegetation land. Similarly, for vegetation, RMB is -2.57%, which is better than other land classes. This may be due to the fact that SREM's estimated surface reflectance over vegetation land was not overestimated as much as other land classes, which results in higher AOD values relative to other classes (Bilal et al., 2022). This study showcases the dependable performance of the AOD retrieval approach of SEMARA in a highly polluted city Kanpur, India.

5.3 Validation of retrieved AOD for cropped and harvested months over different land classes

In this part, we carry out an analysis of the AOD retrievals across all four land classes during two distinct agricultural periods: the cropped periods encompassing between January and mid-April, as well as from August to mid-October. The harvested periods spanning from mid-April to August and mid-October to December. When comparing the retrieved AOD with downscaled MODIS AOD, the correlation was found to be stronger during the harvested period in contrast to the cropped period (Fig. 9). This difference in discrepancy might be attributed to the higher prevalence of brighter surfaces during the harvested period compared to the cropped period. The improved performance of the SEMARA algorithm on brighter surfaces could contribute to this observed pattern. During the harvested period, for the barren and built-up

land class, the SEMARA-retrieved AOD demonstrated the closest match with the MODIS downscaled AOD, showcasing the most favourable agreement between the two datasets.

5.4 Efficiency evaluation for multiple aerosol loadings

The different aerosol loading in the atmospheric column has been proven in several studies to have an impact on the AOD retrieval accuracy (Bilal et al., 2017; Gupta et al., 2013). In this section, we have investigated the performance of the SEMARA approach over four AOD ranges: (i) AOD ≤ 0.25; (ii) 0.25 < AOD ≤ 0.50; (iii) 0.50 < AOD ≤ 0.75; and (iv) AOD > 0.75. Basic statistics for all four ranges have been shown in Table 5, which shows the SEMARA approach has performed better for the midranges of AOD than that of the lower and higher ranges of AOD.

Table 5
Statistics of MODIS and SEMARA derived AOD's for different ranges of AOD loadings over Kanpur region.

	AOD ≤ 0.25		**0.25 < AOD ≤ 0.50**		**0.50 < AOD ≤ 0.75**		**AOD > 0.75**	
	MODIS	SEMARA	MODIS	SEMARA	MODIS	SEMARA	MODIS	SEMARA
Mean	0.3880	0.2248	0.5036	0.4051	0.6079	0.6111	0.6434	0.8556
Median	0.3890	0.2381	0.4798	0.4210	0.5672	0.5899	0.6120	0.8295
Std. dev.	0.1377	0.0253	0.2195	0.0689	0.2714	0.0693	0.2752	0.0770

Figure 10 demonstrates that moderate range SEMARA retrieved AOD better match MAIAC AODs (Fig. 10(b-c)). In contrast to the moderate range of AOD ranges, lower AOD loading (AOD ≤ 0.25) and higher AOD loading (AOD > 0.75) did not correspond (Fig. 10(a) and (d)). Because surface reflectance makes a relatively substantial contribution to the top-of-atmosphere reflectance under low aerosol conditions, inaccuracies in surface reflectance calculation can have a significant impact on the retrieval of AOD (Bilal et al., 2022). In contrast, for higher aerosol loading, the contribution of aerosol is relatively higher than the surface reflectance, which affects the AOD retrieval significantly (Bilal et al., 2021; Gupta et al., 2016).

Table 6 shows that there were very few observations (N = 23) of lower AOD pixels (AOD ≤ 0.25) for most of the days, which shows less accuracy than other ranges of aerosol loadings. The SEMARA approach proved to be most efficient for the AOD range of 0.50–0.75, around 60.4% of the observations fall within the EE envelope for this range, with a RMSE of 0.24 and a MAE of 0.172.

Since there was only a very limited sample size available for validation for low aerosol values, modest RMSE (0.21) and MAE (0.18) for the low range of AOD were found in SEMARA AOD retrievals. In Table 6, we can see that the accuracy of the SEMARA approach is directly affected by the sample size. It is recommended to validate these ranges with a sufficient number of collocation points for future research, it may provide an improved picture of the result.

Table 6
Validation statistics of SEMARA retrieved AOD with MODIS AOD product for different aerosol loading ranges. N denotes the number of collocations.

	AOD ≤ 0.25	0.25 < AOD ≤ 0.50	0.50 < AOD ≤ 0.75	AOD > 0.75
N	23	42	53	52
R	0.4319	0.5280	0.5938	0.6128
RMSE	0.2079	0.2160	0.2370	0.3174
R^2	0.1865	0.2787	0.3526	0.3755
Within EE	21.7391	52.3810	60.3774	42.3077
MAE	0.1789	0.1629	0.1720	0.2596
FOE	-1.0873	-0.3468	0.4876	1.8004

6 Conclusion

The retrieval of high-resolution AOD over a polluted city in the Indo-Gangetic Plain (IGP) using the SEMARA algorithm for the Landsat 8 green band and validation with available in situ and satellite observations is the focus of this study. This algorithm provided AOD for a spatial resolution of 30m, which was applied over the Kanpur region. Retrieved AOD gives a good estimation with AERONET observations. It was observed that the SEMARA algorithm is reliable for further study to retrieve high-resolution AOD over the Indo-Gangetic region. Furthermore, the comparison with downscaled MODIS AOD revealed that the accuracy of the retrieved AOD was notably higher for bright surfaces during the harvested periods. The SEMARA-retrieved AOD exhibited a closer alignment with MODIS downscaled AOD within the moderate AOD ranges, indicating a more precise coincidence between the two datasets. The comparison between the retrieved AOD and the MODIS AOD product did not exhibit as strong a correlation as the comparison with observed AOD data from AERONET. This disparity could potentially arise from the constraints associated with the downscaling methodology employed on the MODIS AOD product. Therefore, researchers may find the SEMARA algorithm to be a more dependable option for high-resolution AOD retrieval in comparison to relying solely on downscaled products.

Declarations

Acknowledgment

The first author of the manuscript, Rohit Kumar Sing gratefully acknowledges the Indian Institute of Technology Kharagpur for conduct of the research work and for UGC, Govt. of India providing research fellowship. The authors are thankful to the USGS Earth resources observational systems (EROS) data centre for freely providing Landsat imagery and MODIS science team for providing MCD19A2 product.

The authors are duly acknowledged and thank the principal investigators of the AERONET site of Kanpur for providing observational AOD dataset.

Declaration of Competing Interest

The authors declare that they have no known competing financial interests or personal relationships that could have appeared to influence the work reported in this paper.

Funding

No funding is available for this work.

Ethics declarations

Conflict of interest: On behalf of all authors, the corresponding author states that there is no conflict of interest.

Authors Contributions

Rohit Kumar Singh and Dr. A.N.V. Satyanarayana contributed to the study conception and design. Material preparation, data collection and analysis were performed by Rohit Kumar Singh and continuously guided by Dr. A.N.V. Satyanarayana. P.S. Hari Prasad contributed in coding and execution of SEMARA algorithm. The first draft of the manuscript was written by Rohit Kumar Singh and corrections and modifications done by Dr. A.N.V. Satyanarayana. All authors read and approved the final manuscript.

Authors Declaration

All authors have read, understood, and have complied as applicable with the statement on "Ethical responsibilities of Authors" as found in the Instructions for Authors

References

1. Acharya, P., & Sreekesh, S. (2013). Seasonal variability in aerosol optical depth over India: a spatio-temporal analysis using the MODIS aerosol product. *International Journal of Remote Sensing*, *34*(13), 4832–4849.
2. Arafath, S. M., Balakrishnaiah, G., Lingaswamy, A. P., & Reddy, R. R. (2015). Columnar-integrated aerosol optical properties and classification of different aerosol types over the semi-arid region, Anantapur, Andhra Pradesh. *Science of the Total Environment*, *527*, 507–519.
3. Bilal, M., Mhawish, A., Ali, M. A., Nichol, J. E., de Leeuw, G., Khedher, K. M., Mazhar, U., Qiu, Z., Bleiweiss, M. P., & Nazeer, M. (2022). Integration of Surface Reflectance and Aerosol Retrieval Algorithms for Multi-Resolution Aerosol Optical Depth Retrievals over Urban Areas. *Remote Sensing*, *14*(2). https://doi.org/10.3390/rs14020373

4. Bilal, M., Nazeer, M., Nichol, J. E., Bleiweiss, M. P., Qiu, Z., Jäkel, E., Campbell, J. R., Atique, L., Huang, X., & Lolli, S. (2019). A simplified and robust surface reflectance estimation method (SREM) for use over diverse land surfaces using multi-sensor data. *Remote Sensing*, *11*(11), 1344.
5. Bilal, M., Nichol, J. E., Bleiweiss, M. P., & Dubois, D. (2013a). A Simplified high resolution MODIS Aerosol Retrieval Algorithm (SARA) for use over mixed surfaces. *Remote Sensing of Environment*, *136*, 135–145.
6. Bilal, M., Nichol, J. E., Bleiweiss, M. P., & Dubois, D. (2013b). A Simplified high resolution MODIS aerosol retrieval algorithm (SARA) for use over mixed surfaces. *Remote Sensing of Environment*, *136*, 135–145. https://doi.org/10.1016/j.rse.2013.04.014
7. Bilal, M., Nichol, J. E., & Spak, S. N. (2017). A new approach for estimation of fine particulate concentrations using satellite aerosol optical depth and binning of meteorological variables. *Aerosol and Air Quality Research*, *17*(2), 356–367.
8. Bilal, M., & Qiu, Z. (2018). Aerosol retrievals over bright urban surfaces using Landsat 8 images. *IGARSS 2018-2018 IEEE International Geoscience and Remote Sensing Symposium*, 7560–7563.
9. Bilal, M., Qiu, Z., Nichol, J. E., Mhawish, A., Ali, M. A., Khedher, K. M., de Leeuw, G., Yu, W., Tiwari, P., & Nazeer, M. (2021). Uncertainty in aqua-modis aerosol retrieval algorithms during covid-19 lockdown. *IEEE Geoscience and Remote Sensing Letters*, *19*, 1–5.
10. Chai, T., & Draxler, R. R. (2014). Root mean square error (RMSE) or mean absolute error (MAE). *Geoscientific Model Development Discussions*, *7*(1), 1525–1534.
11. Chen, C., Li, Z. Q., Hou, W. Z., Li, D. H., & Zhang, Y. H. (2015). Dynamic model in retrieving aerosol optical depth from polarimetric measurements of PARASOL. *J. Remote Sens*, *19*, 25–33.
12. Falah, S., Mhawish, A., Sorek-Hamer, M., Lyapustin, A. I., Kloog, I., Banerjee, T., Kizel, F., & Broday, D. M. (2021). Impact of environmental attributes on the uncertainty in MAIAC/MODIS AOD retrievals: A comparative analysis. *Atmospheric Environment*, *262*, 118659.
13. Ge, J. M., Su, J., Fu, Q., Ackerman, T. P., & Huang, J. P. (2011). Dust aerosol forward scattering effects on ground-based aerosol optical depth retrievals. *Journal of Quantitative Spectroscopy and Radiative Transfer*, *112*(2), 310–319.
14. Gupta, P., Khan, M. N., da Silva, A., & Patadia, F. (2013). MODIS aerosol optical depth observations over urban areas in Pakistan: quantity and quality of the data for air quality monitoring. *Atmospheric Pollution Research*, *4*(1), 43–52.
15. Gupta, P., Levy, R. C., Mattoo, S., Remer, L. A., & Munchak, L. A. (2016). A surface reflectance scheme for retrieving aerosol optical depth over urban surfaces in MODIS Dark Target retrieval algorithm. *Atmospheric Measurement Techniques*, *9*(7), 3293–3308.
16. Gupta, U. (2008). Valuation of urban air pollution: a case study of Kanpur City in India. *Environmental and Resource Economics*, *41*, 315–326.
17. Hadjimitsis, D. G. (2009). Aerosol optical thickness (AOT) retrieval over land using satellite image-based algorithm. *Air Quality, Atmosphere & Health*, *2*, 89–97.

18. Hodson, T. O. (2022). Root-mean-square error (RMSE) or mean absolute error (MAE): When to use them or not. *Geoscientific Model Development*, *15*(14), 5481–5487.
19. Hsu, N. C., Jeong, M., Bettenhausen, C., Sayer, A. M., Hansell, R., Seftor, C. S., Huang, J., & Tsay, S. (2013). Enhanced Deep Blue aerosol retrieval algorithm: The second generation. *Journal of Geophysical Research: Atmospheres*, *118*(16), 9296–9315.
20. Jin, Y., Hao, Z., Chen, J., He, D., Tian, Q., Mao, Z., & Pan, D. (2021). Retrieval of Urban Aerosol Optical Depth from Landsat 8 OLI in Nanjing, China. *Remote Sensing*, *13*(3), 415.
21. Kang, Y., Kim, M., Kang, E., Cho, D., & Im, J. (2022). Improved retrievals of aerosol optical depth and fine mode fraction from GOCI geostationary satellite data using machine learning over East Asia. *ISPRS Journal of Photogrammetry and Remote Sensing*, *183*, 253–268.
22. Karimi, N., Namdari, S., Sorooshian, A., Bilal, M., & Heidary, P. (2019). Evaluation and modification of SARA high-resolution AOD retrieval algorithm during high dust loading conditions over bright desert surfaces. *Atmospheric Pollution Research*, *10*(4), 1005–1014.
23. Kaskaoutis, D. G., Sinha, P. R., Vinoj, V., Kosmopoulos, P. G., Tripathi, S. N., Misra, A., Sharma, M., & Singh, R. P. (2013). Aerosol properties and radiative forcing over Kanpur during severe aerosol loading conditions. *Atmospheric Environment*, *79*, 7–19.
24. Kaufman, Y. J., & Sendra, C. (1988). Algorithm for automatic atmospheric corrections to visible and near-IR satellite imagery. *International Journal of Remote Sensing*, *9*(8), 1357–1381.
25. Koren, I., Altaratz, O., Remer, L. A., Feingold, G., Martins, J. V., & Heiblum, R. H. (2012). Aerosol-induced intensification of rain from the tropics to the mid-latitudes. *Nature Geoscience*, *5*(2), 118–122.
26. Levy, R. C., Mattoo, S., Munchak, L. A., Remer, L. A., Sayer, A. M., Patadia, F., & Hsu, N. C. (2013). The Collection 6 MODIS aerosol products over land and ocean. *Atmospheric Measurement Techniques*, *6*(11), 2989–3034.
27. Levy, R. C., Remer, L. A., Kleidman, R. G., Mattoo, S., Ichoku, C., Kahn, R., & Eck, T. F. (2010). Global evaluation of the Collection 5 MODIS dark-target aerosol products over land. *Atmospheric Chemistry and Physics*, *10*(21), 10399–10420.
28. Liang, T., Liang, S., Zou, L., Sun, L., Li, B., Lin, H., He, T., & Tian, F. (2022). Estimation of Aerosol Optical Depth at 30 m Resolution Using Landsat Imagery and Machine Learning. *Remote Sensing*, *14*(5), 1053.
29. Lin, H., Li, S., Xing, J., He, T., Yang, J., & Wang, Q. (2021). High resolution aerosol optical depth retrieval over urban areas from Landsat-8 OLI images. *Atmospheric Environment*, *261*, 118591.
30. Lyapustin, A., Wang, Y., Korkin, S., & Huang, D. (2018). MODIS Collection 6 MAIAC algorithm. *Atmospheric Measurement Techniques*, *11*(10), 5741–5765. https://doi.org/10.5194/amt-11-5741-2018
31. Mhawish, A., Banerjee, T., Broday, D. M., Misra, A., & Tripathi, S. N. (2017). Evaluation of MODIS Collection 6 aerosol retrieval algorithms over Indo-Gangetic Plain: Implications of aerosols types and mass loading. *Remote Sensing of Environment*, *201*, 297–313.

32. Mhawish, A., Banerjee, T., Sorek-Hamer, M., Lyapustin, A., Broday, D. M., & Chatfield, R. (2019). Comparison and evaluation of MODIS Multi-angle Implementation of Atmospheric Correction (MAIAC) aerosol product over South Asia. *Remote Sensing of Environment*, *224*, 12–28.
33. Mi, W., Li, Z., Xia, X., Holben, B., Levy, R., Zhao, F., Chen, H., & Cribb, M. (2007). Evaluation of the moderate resolution imaging spectroradiometer aerosol products at two aerosol robotic network stations in China. *Journal of Geophysical Research: Atmospheres*, *112*(D22).
34. Murari, V., Kumar, M., Barman, S. C., & Banerjee, T. (2015). Temporal variability of MODIS aerosol optical depth and chemical characterization of airborne particulates in Varanasi, India. *Environmental Science and Pollution Research*, *22*, 1329–1343.
35. Nair, V. S., Moorthy, K. K., Alappattu, D. P., Kunhikrishnan, P. K., George, S., Nair, P. R., Babu, S. S., Abish, B., Satheesh, S. K., & Tripathi, S. N. (2007). Wintertime aerosol characteristics over the Indo-Gangetic Plain (IGP): Impacts of local boundary layer processes and long-range transport. *Journal of Geophysical Research: Atmospheres*, *112*(D13).
36. Payra, S., Gupta, P., Bhatla, R., El Amraoui, L., & Verma, S. (2021). Temporal and spatial variability in aerosol optical depth (550 nm) over four major cities of India using data from MODIS onboard the Terra and Aqua satellites. *Arabian Journal of Geosciences*, *14*(13), 1256.
37. Pope, C. A., Thun, M. J., Namboodiri, M. M., Dockery, D. W., Evans, J. S., Speizer, F. E., & Heath, C. W. (1995). Particulate air pollution as a predictor of mortality in a prospective study of US adults. *American Journal of Respiratory and Critical Care Medicine*, *151*(3), 669–674.
38. Pope III, C. A., Ezzati, M., & Dockery, D. W. (2009). Fine-particulate air pollution and life expectancy in the United States. *New England Journal of Medicine*, *360*(4), 376–386.
39. Rahman, M. M., & Haque, S. (2022). Retrieving spatial variation of aerosol level over urban mixed land surfaces using Landsat imageries: Degree of air pollution in Dhaka Metropolitan Area. *Physics and Chemistry of the Earth, Parts a/b/c*, *126*, 103074.
40. Ramachandran, S., Srivastava, R., Kedia, S., & Rajesh, T. A. (2012). Contribution of natural and anthropogenic aerosols to optical properties and radiative effects over an urban location. *Environmental Research Letters*, *7*(3), 034028.
41. Remer, L. A., Levy, R. C., Mattoo, S., Tanré, D., Gupta, P., Shi, Y., Sawyer, V., Munchak, L. A., Zhou, Y., & Kim, M. (2020). The dark target algorithm for observing the global aerosol system: Past, present, and future. *Remote Sensing*, *12*(18), 2900.
42. Sayer, A. M., Munchak, L. A., Hsu, N. C., Levy, R. C., Bettenhausen, C., & Jeong, M. (2014). MODIS Collection 6 aerosol products: Comparison between Aqua's e-Deep Blue, Dark Target, and "merged" data sets, and usage recommendations. *Journal of Geophysical Research: Atmospheres*, *119*(24), 13–965.
43. Shukla, N., Sharma, G. K., Baruah, P., Shukla, V. K., & Gargava, P. (2020). Impact of shutdown due to COVID-19 pandemic on aerosol characteristics in Kanpur, India. *Journal of Health and Pollution*, *10*(28).

44. Stowe, L. L., Carey, R. M., & Pellegrino, P. P. (1992). Monitoring the Mt. Pinatubo aerosol layer with NOAA/11 AVHRR data. *Geophysical Research Letters*, *19*(2), 159–162.
45. Sultana, S., & Satyanarayana, A. N. V. (2018). Urban heat island intensity during winter over metropolitan cities of India using remote-sensing techniques: Impact of urbanization. *International Journal of Remote Sensing*, *39*(20), 6692–6730.
46. Sultana, S., & Satyanarayana, A. N. V. (2020). Assessment of urbanisation and urban heat island intensities using landsat imageries during 2000–2018 over a sub-tropical Indian City. *Sustainable Cities and Society*, *52*, 101846.
47. Tanré, D., Deschamps, P. Y., Devaux, C., & Herman, M. (1988). Estimation of Saharan aerosol optical thickness from blurring effects in Thematic Mapper data. *Journal of Geophysical Research: Atmospheres*, *93*(D12), 15955–15964.
48. Tao, M., Wang, J., Li, R., Wang, L., Wang, L., Wang, Z., Tao, J., Che, H., & Chen, L. (2019). Performance of MODIS high-resolution MAIAC aerosol algorithm in China: Characterization and limitation. *Atmospheric Environment*, *213*, 159–169.
49. The, D., Burden, G., Air, C., & Agency, E. E. (2018). *WHO's Ambient (Outdoor) Air Quality Database–Update 2018*.
50. Tripathi, S. N., Dey, S., Chandel, A., Srivastava, S., Singh, R. P., & Holben, B. N. (2005). Comparison of MODIS and AERONET derived aerosol optical depth over the Ganga Basin, India. *Annales Geophysicae*, *23*(4), 1093–1101.
51. Van de Hulst, H. C. (1948). Scattering in a planetary atmosphere. *Astrophysical Journal*, 107–220.
52. Wei, J., Huang, B., Sun, L., Zhang, Z., Wang, L., & Bilal, M. (2017). A simple and universal aerosol retrieval algorithm for Landsat series images over complex surfaces. *Journal of Geophysical Research: Atmospheres*, *122*(24), 13–338.
53. Zhang, Y., Wang, J., & Bu, L. (2019). Analysis of a haze event over Nanjing, China based on multi-source data. *Atmosphere*, *10*(6), 338.

Figures

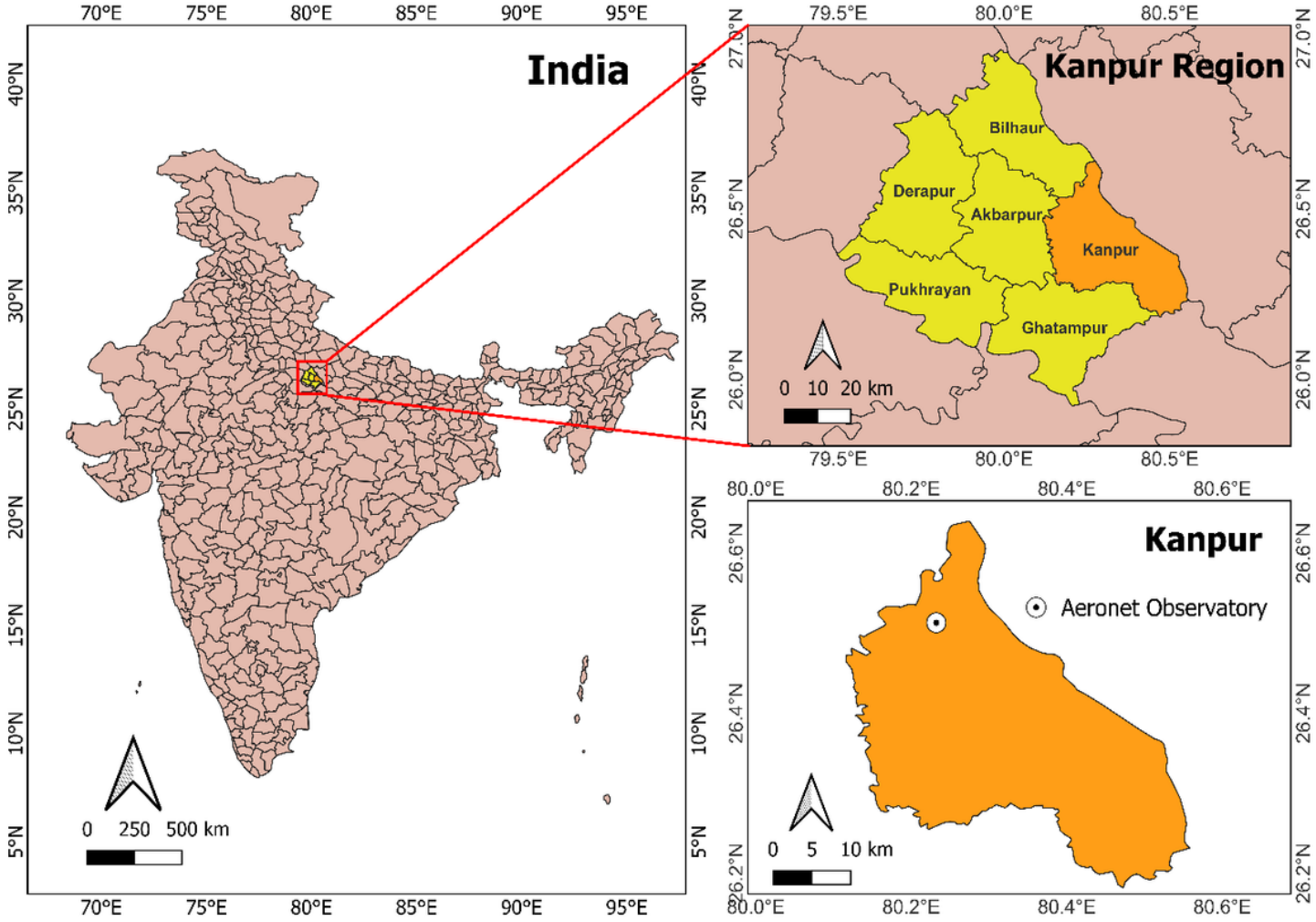

Figure 1

Study Area

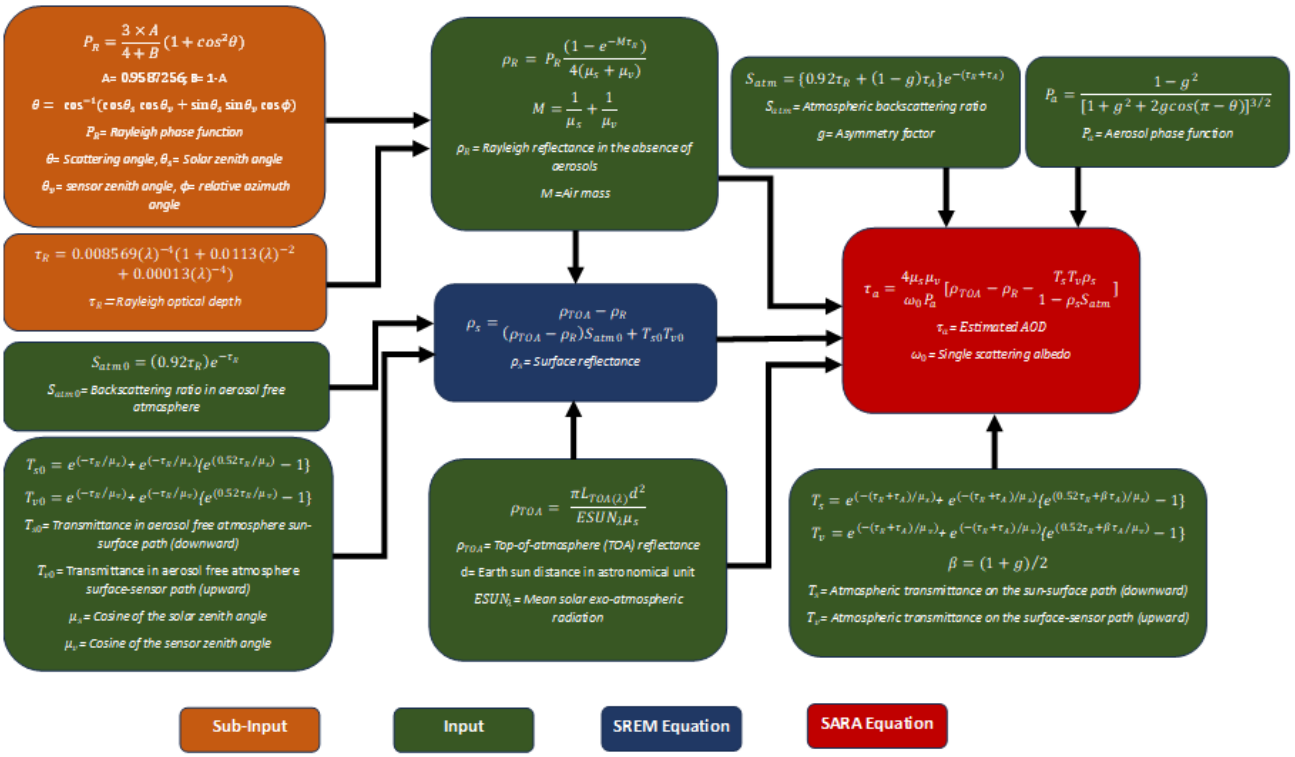

Figure 2

A methodological procedure used in the SEMARA method to retrieve AOD, which integrates the SARA (Bilal et al., 2013a) and SREM (Bilal et al., 2019) algorithms.

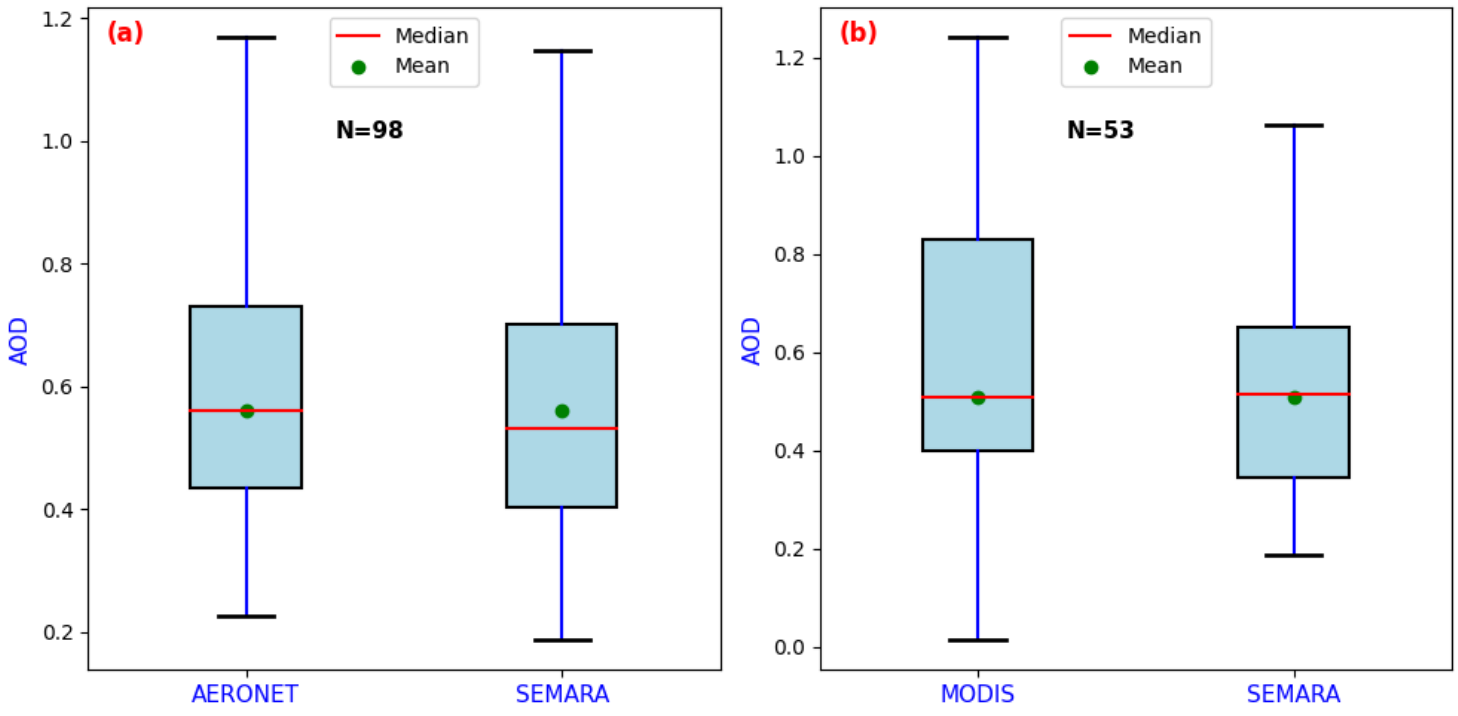

Figure 3

Box plot showing comparison between SEMARA retrieved AOD and (a) AERONET point observations and (b) MODIS satellite AOD product.

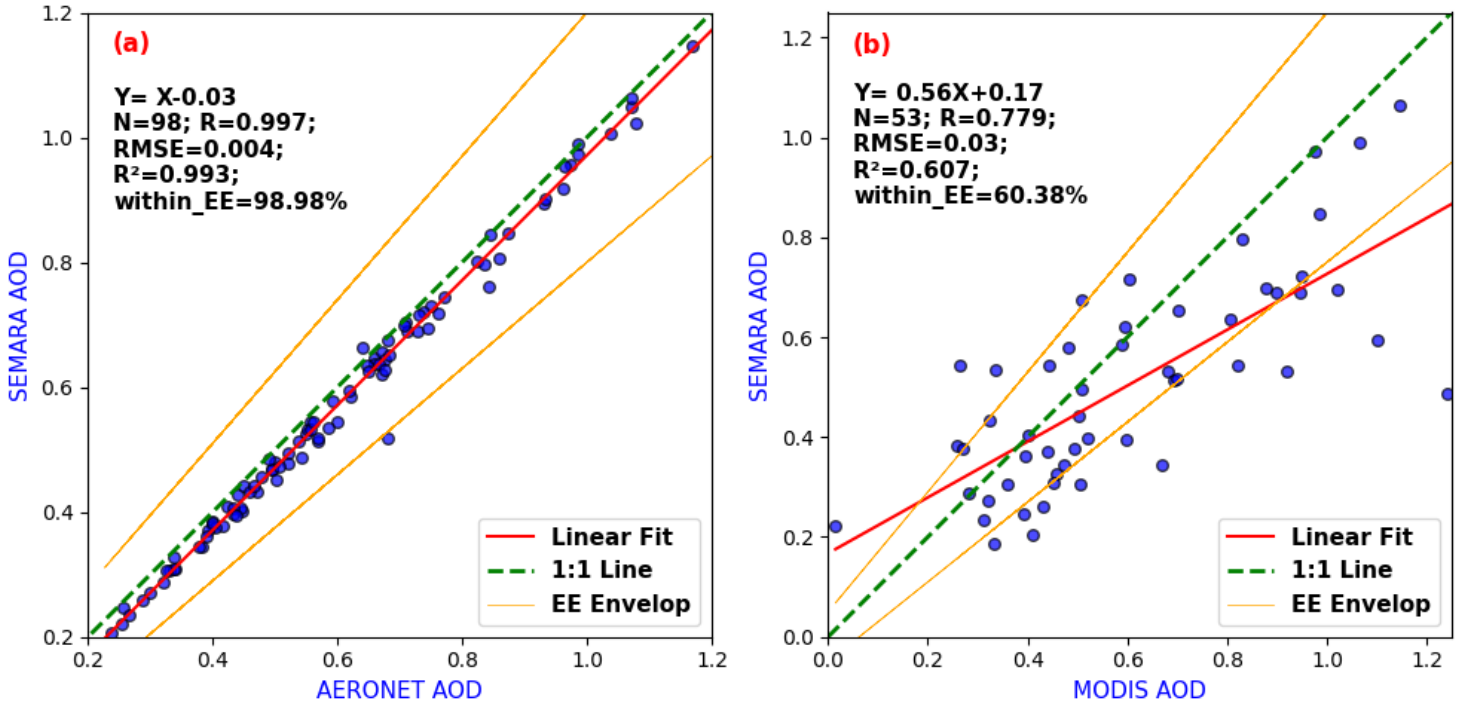

Figure 4

Validation of SEMARA retrieved AOD with (a) AERONET observations and (b) MODIS MAIAC product.

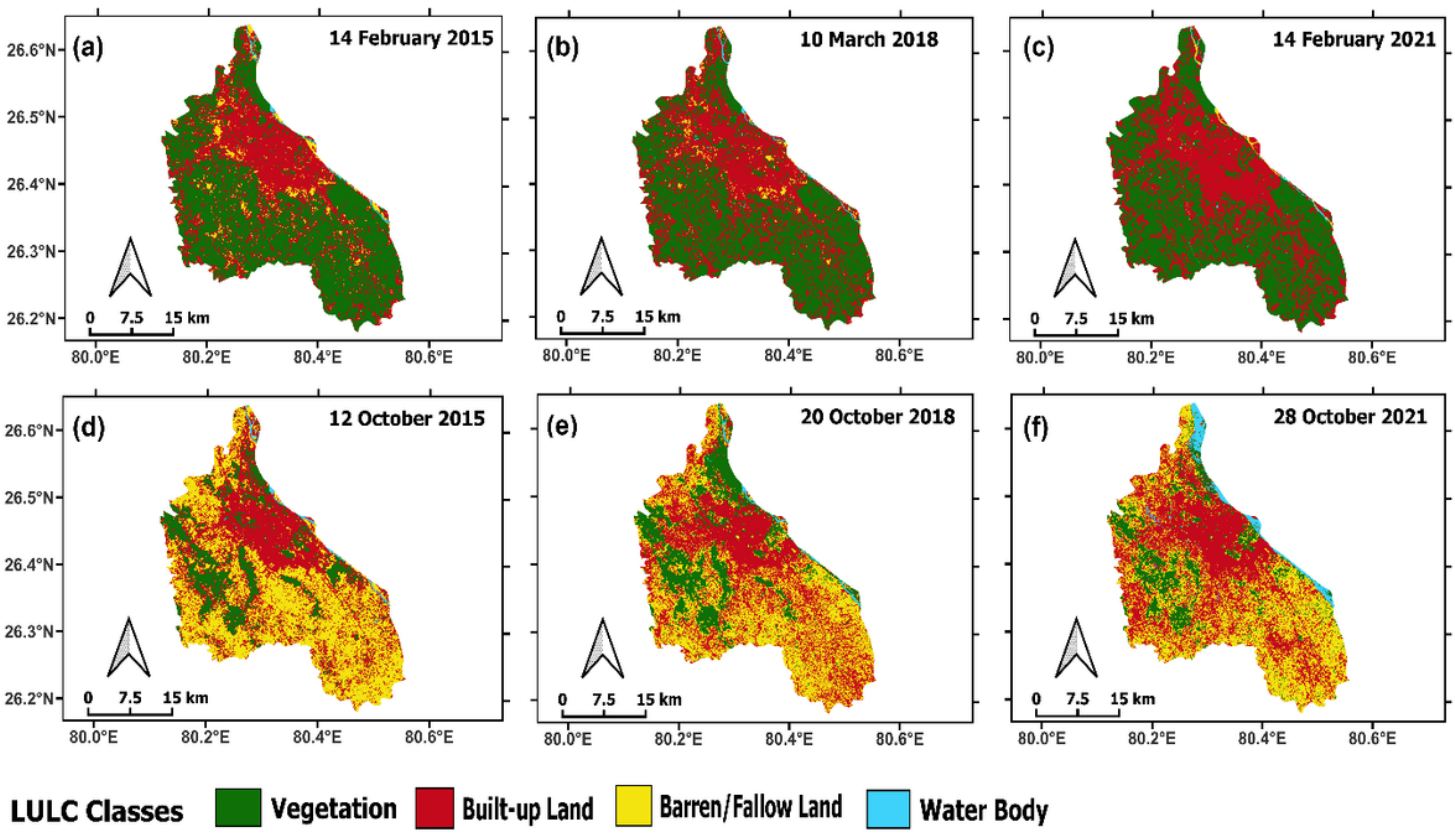

Figure 5

Land use land classification map for Kanpur region for cropped ((a)-(c)) and harvested months ((d)-(f)).

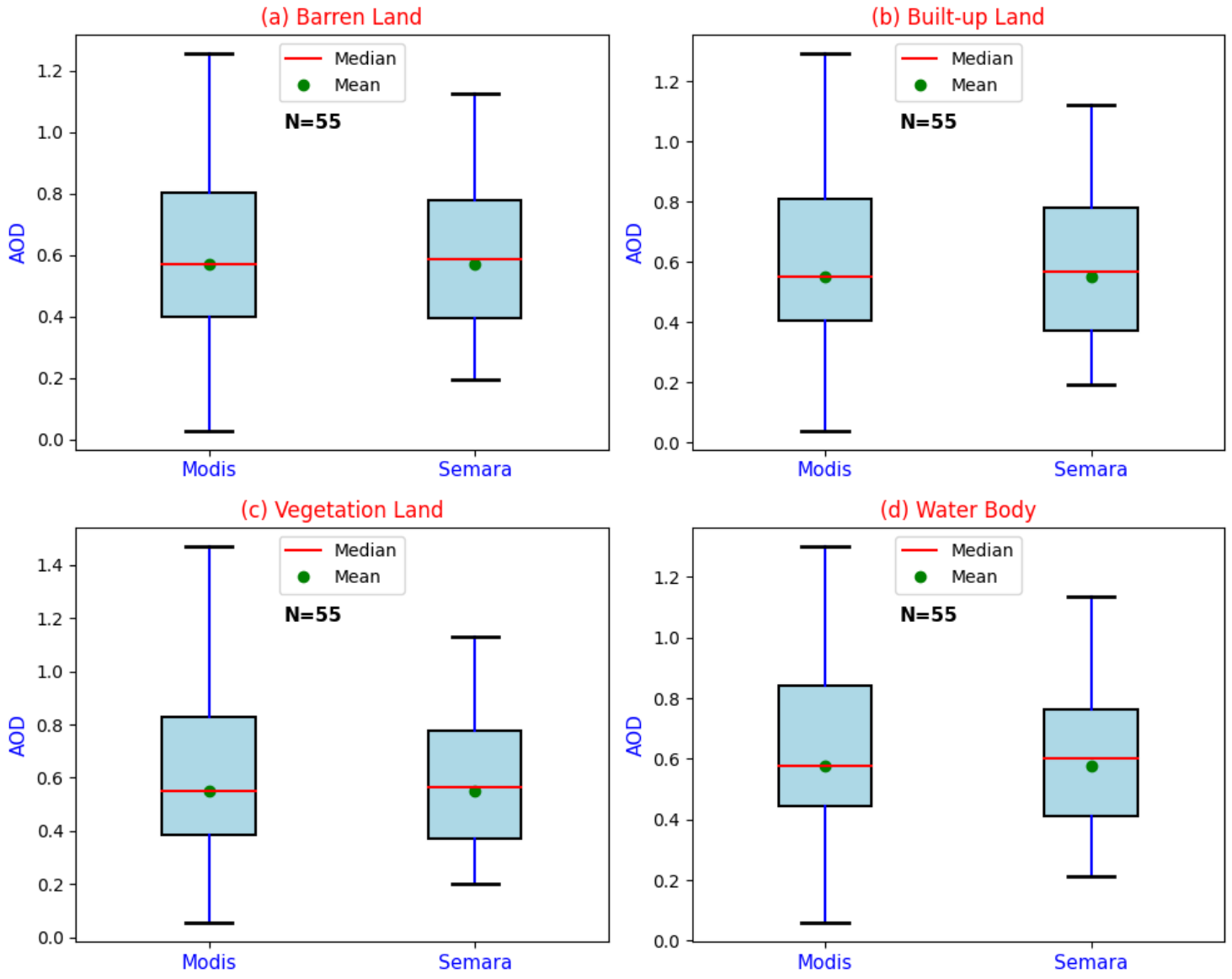

Figure 6

Plot shows the variation and central tendency of retrieved AOD and available MODIS AOD product for four land classes.

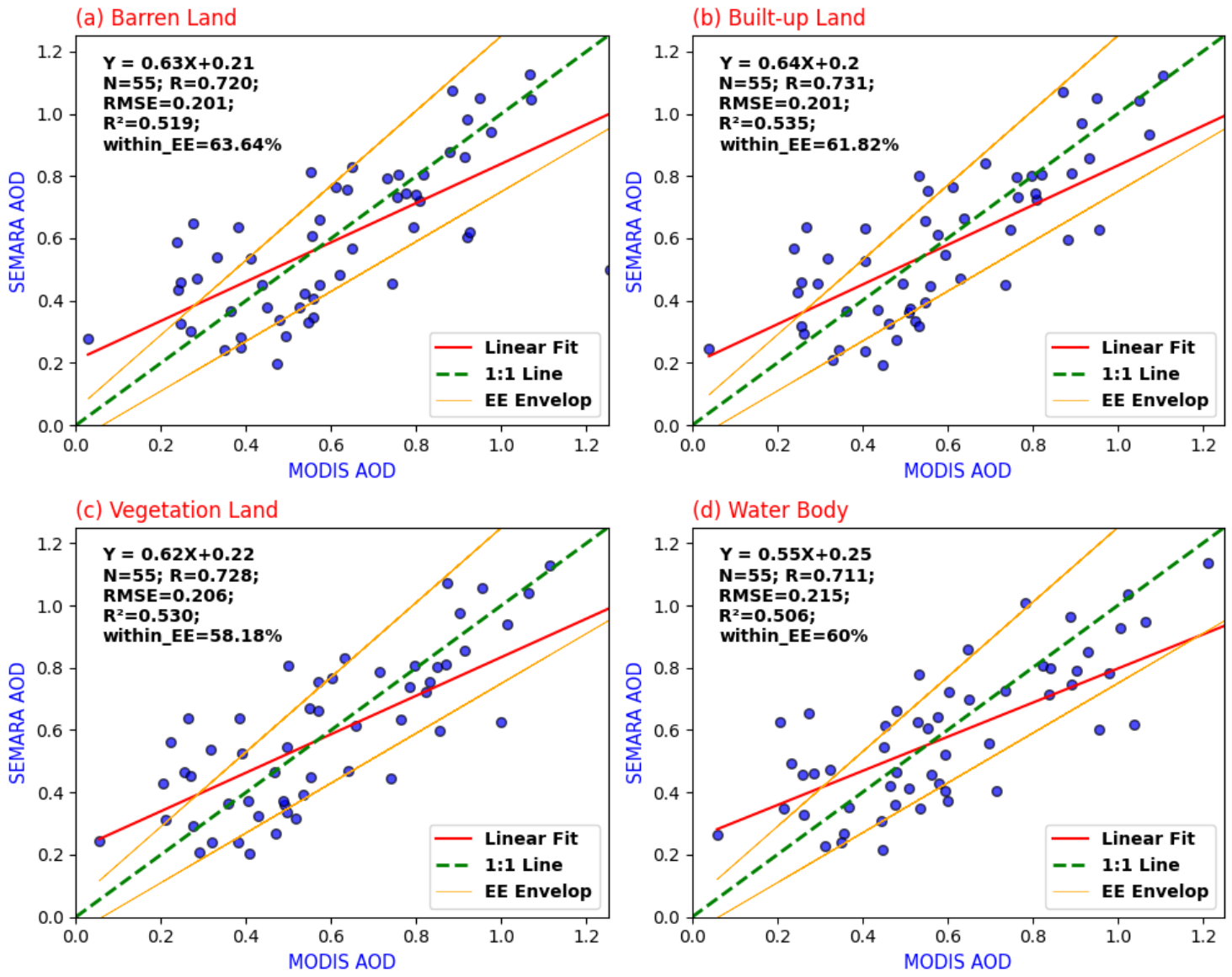

Figure 7

Validation of SEMARA derived AOD with MODIS AOD product for land classes of (a) Barren Land, (b) Built-up Land, (c) Vegetation Land, and (d) Water Body.

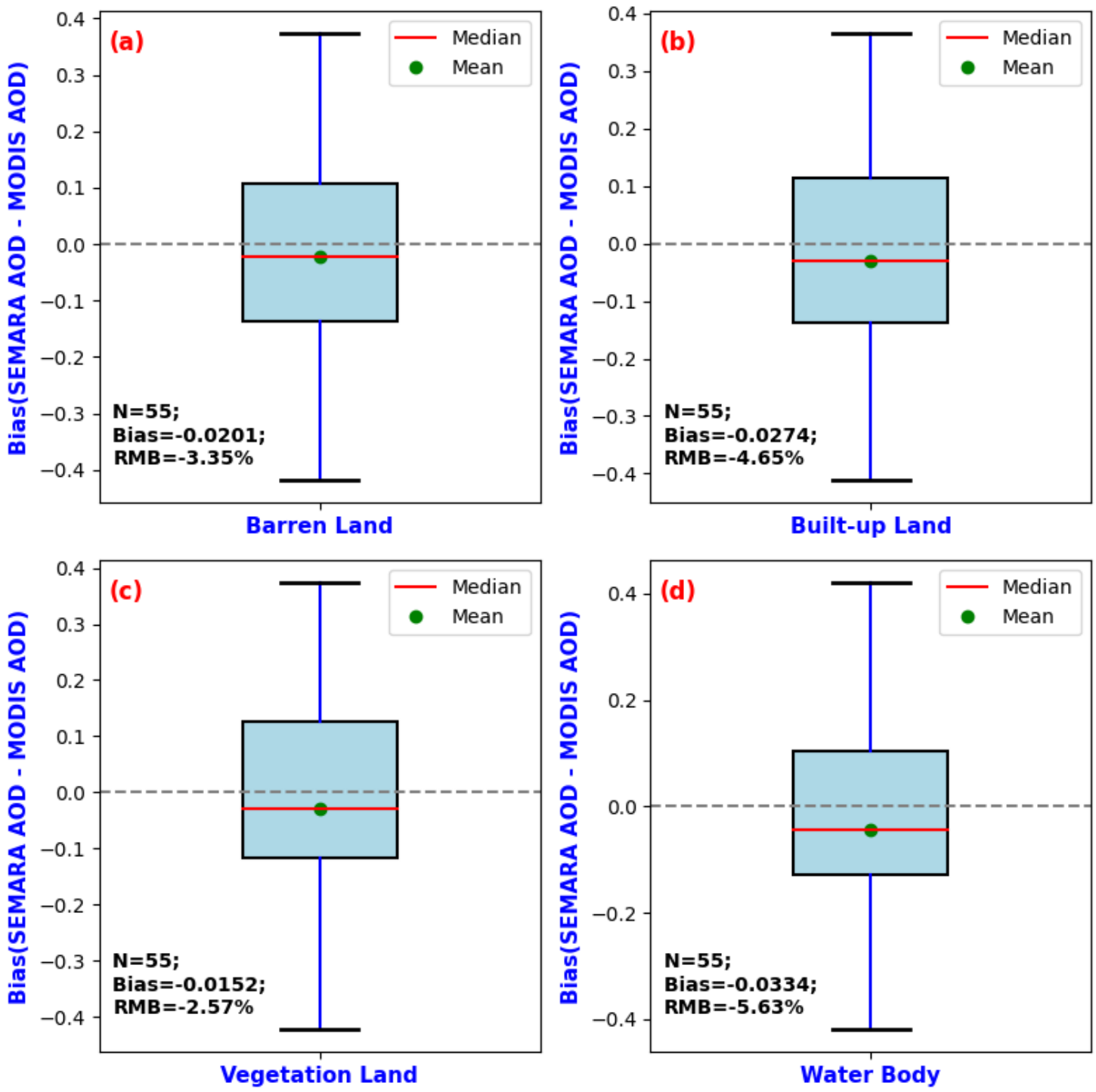

Figure 8

Box plots showing bias of SEMARA and MODIS retrieved AOD for the land classes of (a) Barren Land, (b) Built-up Land, (c) Vegetation and (d) Water Body.

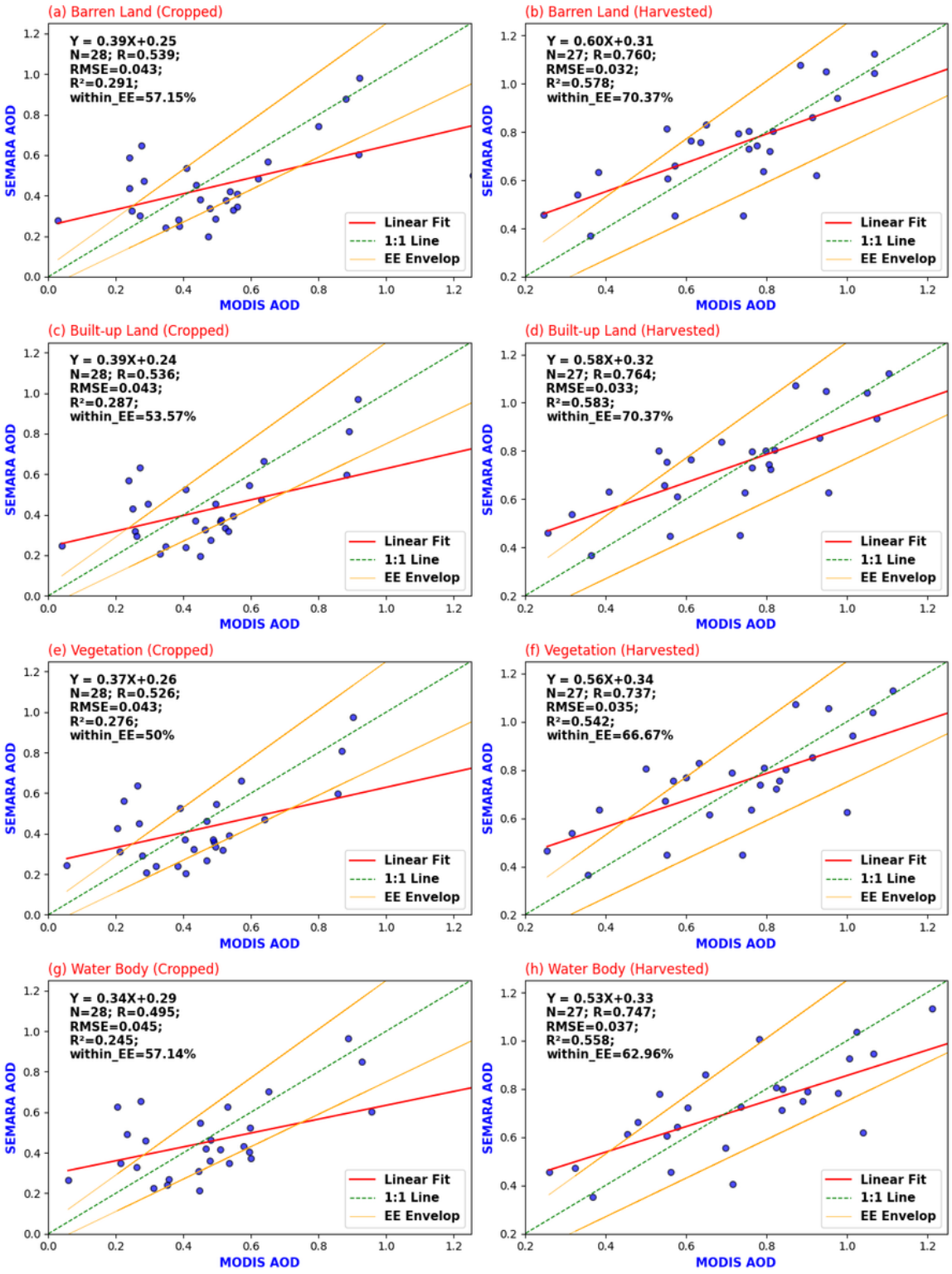

Figure 9

Validation of retrieved AOD with MODIS AOD product based on land cover type for cropped and harvested agricultural cycle.

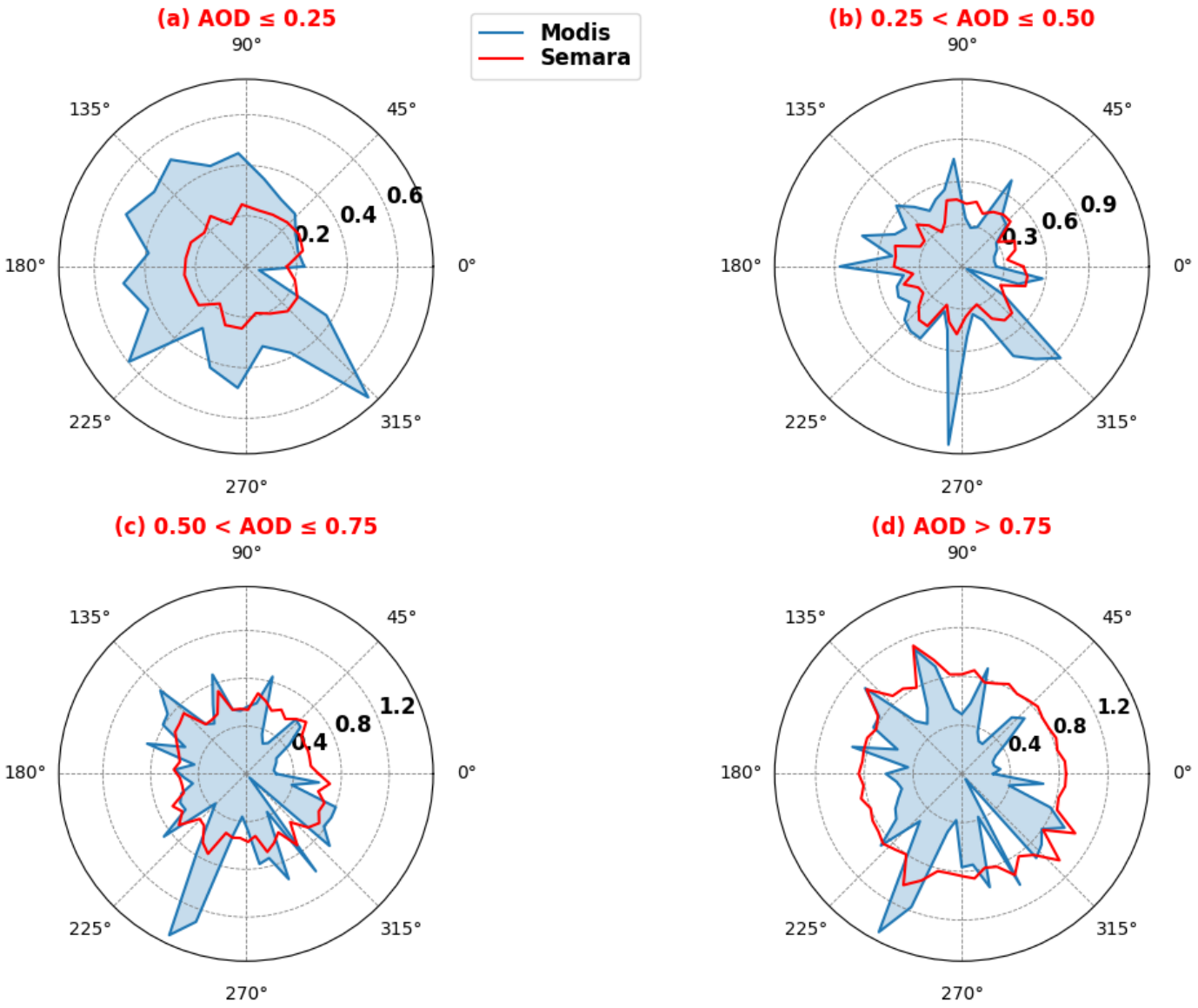

Figure 10

Radar plots show the performance of SEMARA retrieved AOD with respect to MODIS derived AOD for four AOD ranges of (a) AOD ≤ 0.25, (b) 0.25 < AOD ≤ 0.50, (c) 0.50 < AOD ≤ 0.75, and (d) AOD > 0.75.